

# Dilepton emission rates from hot hadronic matter

Thorsten Renk\*

*Physik Department, Technische Universität München, D - 85745, Garching, Germany*

Amruta Mishra†

*Institut für Theoretische Physik, Robert Mayer Str. 8-10,*

*D-60054 Frankfurt am Main, Germany*

(Dated: February 9, 2020)

## Abstract

The vacuum polarisation effects from the nucleon sector lead to large medium modifications of the vector meson masses in the Walecka model. With a quantum hydrodynamic framework including the quantum effects, and using a quasiparticle description for quark gluon plasma(QGP), the dilepton emission rate from the hot and dense matter resulting from relativistic nuclear collisions is calculated. Using a model for the fireball evolution which has been shown to reproduce other observables such as charmonium suppression, photon emission and the abundance of hadronic species, we compare with the dilepton invariant mass spectrum measured by the CERES collaboration at CERN SPS. We also compare the results to a previous calculation where the spectral function of a virtual photon (a key ingredient for the emission rate) has been calculated in a chiral SU(3) model.

---

\*Electronic address: [trenk@physik.tu-muenchen.de](mailto:trenk@physik.tu-muenchen.de)

†Electronic address: [mishra@th.physik.uni-frankfurt.de](mailto:mishra@th.physik.uni-frankfurt.de)

## 1. INTRODUCTION

The study of the in-medium properties of the vector mesons ( $\rho$  and  $\omega$ ) in hot and dense matter is actively investigated, both experimentally [1, 2] and theoretically [3, 4]. The experimental observation of enhanced dilepton production [1] in the low invariant mass regime possibly is due to a reduction in the vector meson masses in the medium. It was first suggested by Brown and Rho that the vector meson masses drop in the medium according to a simple scaling law [3]. Within the framework of Quantum Hadrodynamics (QHD), the vacuum polarisation effects from the baryon sector [5, 6, 7, 8] lead to a significant drop of the vector meson masses in the medium whereas the mass modification is marginal with only Fermi sea polarisation effects. The properties of the hadrons as modified in the thermal bath are reflected in the dilepton and photon spectra emitted from a hot and dense matter [8, 9, 10]. Dileptons are interesting probes for the study of the hot and dense matter formed in relativistic heavy ion collisions. Since they do not interact strongly, the dileptons escape unthermalized from the hot and dense matter at all stages of the evolution. The observed enhancement of dileptons in the low invariant mass regime has initiated extensive theoretical investigations on the temperature [11] and density [12] modifications of the dileptons from hot hadronic matter as well as from a quark gluon plasma (QGP) formed in heavy ion collisions. The increased dilepton yield in S+Au collisions as observed by the CERES collaboration was attributed to enhanced  $\rho$ -meson production via  $\pi^+\pi^-$  annihilation and a dropping of the  $\rho$ -mass in the medium [13, 14]. A large broadening of the  $\rho$ -meson spectral function arising due to scattering off by baryons [15, 16] has been shown to reproduce the CERES data quite well. In the present investigation, the space-time evolution of the strongly compressed hadronic matter formed in a relativistic heavy ion collision is considered in a mixed scenario of QGP and hadronic matter. The QGP is described within a quasiparticle picture [17] and the hadronic matter described in a Quantum Hadrodynamics framework including quantum fluctuation effects from the baryon and scalar meson sectors [18, 19, 20]. The dilepton emission rates from the expanding fireball are then studied in a model based on local thermal equilibrium and isentropic expansion [21].

It was earlier demonstrated in a nonperturbative formalism that a realignment of the ground state with baryon-antibaryon condensates is equivalent to the relativistic Hartree approximation (RHA) [18]. The ground state for the nuclear matter was extended to include

sigma condensates to take into account the quantum correction effects from the scalar meson sector [18]. Such a formalism includes multiloop effects and is self consistent [18, 22]. The methodology was then generalized to consider hot nuclear matter [23] as well as to study hyperon-rich dense matter [24] relevant for neutron stars. The effect of vacuum polarisations on the vector meson properties [19] and on the static dilepton spectra [20] has also been recently studied. In the low invariant mass regime, the scalar meson contributions lead to considerable broadening the  $\omega$  peak in the dilepton spectra as compared to RHA, which leads to smearing and ultimate disappearance of the  $\omega$  peak at high densities [20]. The present investigation of dilepton spectra using a dynamical fireball model is compared with results obtained using other descriptions for hadronic matter [13, 16], as well as to the experimental results from CERES collaboration [1].

We organize the paper as follows. We first briefly recapitulate the nonperturbative framework used for studying the medium modification of the  $\omega$  and  $\rho$  vector meson properties including the vacuum fluctuation effects in the Walecka model, in section 2. Section 3 discusses the parametrisation of the photon self energy in the hadronic phase. The quark gluon plasma (QGP) phase is treated within a quasiparticle picture [17] as described in section 4. In section 5, we describe briefly the model considered for the dynamical evolution of the fireball. Section 6 deals with the calculation of dilepton emission from the fireball. Finally, we discuss the findings of the present investigation in section 7 and summarise in section 8.

## **2. VACUUM POLARISATION EFFECTS AND IN-MEDIUM VECTOR MESON PROPERTIES**

We briefly recapitulate here the vacuum polarisation effects arising from the nucleon and scalar meson fields in hot nuclear matter in a nonperturbative variational framework [23] and their influence on the vector meson properties in the hot and dense matter. The method of thermofield dynamics (TFD) [25] is used here to study the “ground state” (the state with minimum thermodynamic potential) at finite temperature and density within the Walecka model with a quartic scalar self interaction. The temperature and density dependent baryon and sigma masses are also calculated in a self-consistent manner in the formalism. The ansatz functions involved in such an approach are determined through functional minimisation of the thermodynamic potential.

The Lagrangian density in the Walecka model is given as

$$\begin{aligned} \mathcal{L} = & \bar{\psi} (i\gamma^\mu \partial_\mu - M - g_\sigma \sigma - g_\omega \gamma^\mu \omega_\mu) \psi + \frac{1}{2} \partial^\mu \sigma \partial_\mu \sigma - \frac{1}{2} m_\sigma^2 \sigma^2 - \lambda \sigma^4 \\ & + \frac{1}{2} m_\omega^2 \omega^\mu \omega_\mu - \frac{1}{4} (\partial_\mu \omega_\nu - \partial_\nu \omega_\mu) (\partial^\mu \omega^\nu - \partial^\nu \omega^\mu). \end{aligned} \quad (1)$$

In the above,  $\psi$ ,  $\sigma$ , and  $\omega_\mu$  are the fields for the nucleon,  $\sigma$ , and  $\omega$  mesons with masses  $M$ ,  $m_\sigma$ , and  $m_\omega$  respectively. The quartic coupling term in  $\sigma$  is necessary for the sigma condensates to exist, through a vacuum realignment [18]. Our calculations thus include the quantum effects arising from the sigma meson in addition to the mean field contribution from the the quartic self interaction of the scalar meson. We retain the quantum nature of both the nucleon and the scalar meson fields, whereas the vector  $\omega$ - meson is treated as a classical field, which in the mean field approximation is given as  $\langle \omega^\mu \rangle = \delta_{\mu 0} \omega_0$ . The reason is that without higher-order term for the  $\omega$ -meson, the quantum effects generated due to the  $\omega$ -meson through the present variational ansatz turn out to be zero. The thermodynamic quantities including the quantum effects can then be written down. The details regarding the formalism can be found in earlier references [18, 19, 23]. Extremisation of the thermodynamic potential, with respect to the meson fields  $\sigma_0$  and  $\omega_0$  yields the self-consistency conditions for  $\sigma_0$  (and hence for the effective nucleon mass,  $M^* = M + g_\sigma \sigma_0$ ), and for the vector meson field  $\omega_0$ . We might note here that the quantum effects arising from the scalar meson sector through  $\sigma$  meson condensates amount to a sum over a class of multiloop diagrams and, do not correspond to the one meson loop approximation for scalar meson quantum effects considered earlier [26].

### 2.1. In-medium vector meson masses

We now examine the medium modification to the masses of the  $\omega$ - and  $\rho$ -mesons in hot nuclear matter including the quantum correction effects in the relativistic random phase approximation. The interaction vertices for these mesons with nucleons are given as

$$\mathcal{L}_{\text{int}} = g_V \left( \bar{\psi} \gamma_\mu \tau^a \psi V_a^\mu - \frac{\kappa_V}{2M_N} \bar{\psi} \sigma_{\mu\nu} \tau^a \psi \partial^\nu V_a^\mu \right) \quad (2)$$

where  $V_a^\mu = \omega^\mu$  or  $\rho_a^\mu$ ,  $M_N$  is the free nucleon mass,  $\psi$  is the nucleon field and  $\tau_a = 1$  or  $\vec{\tau}$ ,  $\vec{\tau}$  being the Pauli matrices.  $g_V$  and  $\kappa_V$  correspond to the couplings due to the vector and tensor interactions for the corresponding vector mesons to the nucleon fields. The vector

meson self energy is expressed in terms of the nucleon propagator,  $G(k)$  modified by the quantum effects. This is given as

$$\Pi^{\mu\nu}(k) = -\gamma_I g_V^2 \frac{i}{(2\pi)^4} \int d^4p \text{Tr} \left[ \Gamma_V^\mu(k) G(p) \Gamma_V^\nu(-k) G(p+k) \right], \quad (3)$$

where  $\gamma_I = 2$  is the isospin degeneracy factor for nuclear matter, and  $\Gamma_V^\mu(k) = \gamma^\mu \tau_a - \frac{\kappa_V}{2M_N} \sigma^{\mu\nu}$  represents the meson-nucleon vertex function. For the  $\omega$  meson, the tensor coupling, being small as compared to the vector coupling to the nucleons [6], is neglected [19, 20]. After carrying out the renormalization procedures for the vector self energies, the effective mass of the vector meson is obtained by solving the equation

$$k_0^2 - m_V^2 + \text{Re}\Pi(k_0, \mathbf{k} = 0) = 0. \quad (4)$$

where  $\Pi = \frac{1}{3} \Pi_\mu^\mu$ .

## 2.2. Meson decay properties

For a baryon-free environment,  $\rho \rightarrow \pi^+ \pi^-$  is the dominant decay channel for  $\rho$  meson. The decay width for this process is calculated from the imaginary part of the self energy using the Cutkosky rule, and in the rest frame of the  $\rho$ -meson is given by

$$\Gamma_\rho(k_0) = \frac{g_{\rho\pi\pi}^2}{48\pi} \frac{(k_0^2 - 4m_\pi^2)^{3/2}}{k_0^2} \left[ \left(1 + f\left(\frac{k_0}{2}\right)\right) \left(1 + f\left(\frac{k_0}{2}\right)\right) - f\left(\frac{k_0}{2}\right) f\left(\frac{k_0}{2}\right) \right] \quad (5)$$

where,  $f(x) = [e^{\beta x} - 1]^{-1}$  is the Bose-Einstein distribution function. The first and the second terms in the equation (5) correspond to the decay and the formation of the resonance,  $\rho$ . In the calculation for the  $\rho$  decay width, the pion has been treated as free, and any modification of the pion propagator due to effects like delta-nucleon hole excitation [27] to yield a finite decay width for the pion, have not been taken into account. The coupling  $g_{\rho\pi\pi}$  is fixed from the decay width of  $\rho$  meson in vacuum ( $\Gamma_\rho=151$  MeV) decaying to two pions.

In the presence of baryons, however, it has been shown that there is considerable increase of the  $\rho$  decay width [16] in the thermal medium due to the scattering off the baryons. The dominant contributions which lead to appreciable broadening of the  $\rho$ - spectral function are the inelastic processes  $\rho N \rightarrow \pi N$  and  $\rho N \rightarrow \pi \Delta$ . The imaginary parts of the corresponding scattering amplitudes in the large baryon mass limit are given as [16]

$$\text{Im}\Gamma_{\rho N}^{(\pi N)} = g_A^2 \mathcal{H}(k_0, 0, m_\pi) \quad (6)$$

and

$$\text{Im}T_{\rho N}^{(\pi\Delta)} = 2g_A^2 \mathcal{H}(k_0, m_\Delta^* - m_N^*, m_\pi) \quad (7)$$

where,

$$\begin{aligned} \mathcal{H}(k_0, \Delta, m) = & \frac{g_{\rho NN}^2}{6\pi f_\pi^2} \left[ \frac{\sqrt{(k_0 - \Delta)^2 - m^2}}{(k_0^2 - 2k_0\Delta)^2} (3k_0^4 - 4k_0^2 m^2 + 4m^4 + \Delta(8k_0 m^2 - 12k_0^3)) \right. \\ & + \Delta^2(16k_0^2 - 8m^2) - 8\Delta^3 k_0 + 4\Delta^4 \\ & \left. - \frac{\Delta(k_0^2 - 4m^2)^{3/2}}{2k_0(k_0^2 - 4\Delta^2)^2} (3k_0^2 - 8m^2 - 4\Delta^2) \right] \quad (8) \end{aligned}$$

In the above,  $g_A$  is the axial vector coupling constant chosen to be  $g_A = 1.26$  [16]. The  $\rho NN$  coupling is as fitted from the  $NN$  scattering data [28] and is given as  $g_{\rho NN}=2.6$ . We might note that, by definition, the  $\rho NN$  coupling used here is half of the coupling in Ref [16].

For high energies, the  $\rho N$  scattering process,  $\rho N \rightarrow \omega N$  also becomes important [16]. The corresponding scattering amplitude is given as

$$ImT_{\rho N}^{(\pi\omega)} = \frac{g_A^2 g_{\omega\rho\pi}^2}{48\pi f_\pi^2 m_\pi^2} \frac{k_0^2 \vec{k}_\omega^3 \left[ 2k_\omega^2 m_N^{*2} - m_N^* (k_{\omega 0} - k_0) [(k_{\omega 0} - k_0)^2 - \vec{k}_\omega^2] \right]}{m_N^* (m_N^* + k_0) (m_\pi^2 - m_\omega^{*2} + 2k_{\omega 0} k_0 - k_0^2)^2} \quad (9)$$

The interaction Lagrangian describing  $\omega\rho\pi$  as used above, is given as [30]

$$\mathcal{L}_{\omega\rho\pi} = \frac{g_{\omega\rho\pi}}{m_\pi} \epsilon_{\mu\nu\alpha\beta} \partial^\mu \omega^\nu \partial^\alpha \rho_i^\beta \pi_i \quad (10)$$

For the  $\omega\rho\pi$  coupling we take the value  $g_{\omega\rho\pi} = 2$  according to Ref. [8] consistent with the decay width of  $\omega \rightarrow \pi\gamma$ . The  $\omega\rho\pi$  coupling as here is similar to that used in [31] after accounting for a factor of  $m_\pi/f_\pi$  difference in the definitions. In the above,  $|\vec{k}_\omega| = \sqrt{\lambda(m_N^* + k_0, m_\omega^*, m_N^*)}/(2(m_N^* + k_0))$  and  $k_{\omega 0} = \sqrt{m_\omega^{*2} + \vec{k}_\omega^2}$ . The Källén function  $\lambda$  is defined by  $\lambda(x, y, z) = (x^2 - (y + z)^2)(x^2 - (y - z)^2)$ . The present calculations for the collisional decay width of  $\rho$  meson take into account the mass modifications of the nucleon and vector mesons ( $\rho$  and  $\omega$ ). For  $\Delta$ , we assume that the mass scales in the same way as the nucleon mass in the medium, with  $m_\Delta=1232$  MeV as the mass in vacuum.

The contribution to the decay width of  $\rho$  due to  $\rho N$  scattering processes, arising from the  $\pi N$ ,  $\pi\Delta$  and  $\omega\pi$  loops are given in terms of the imaginary parts of the scattering amplitudes as [16]

$$\Gamma_{\rho N}^{coll} = \frac{\rho_B (ImT_{\rho N}^{(\pi N)} + ImT_{\rho N}^{(\pi\Delta)} + ImT_{\rho N}^{(\omega\pi)})}{k_0} \quad (11)$$

We might note here that the effect of  $\rho N$  scattering on the real part of the scattering amplitude has been seen to be negligible [16] and has not been considered here.

To calculate the decay width for the  $\omega$ -meson, we write down the effective Lagrangian for the  $\omega$  meson as [29, 30]

$$\mathcal{L}_\omega = -\frac{em_\omega^2}{g_\omega}\omega^\mu A_\mu + \frac{g_{\omega 3\pi}}{m_\pi^3}\epsilon_{\mu\nu\alpha\beta}\epsilon_{ijk}\omega^\mu\partial^\nu\pi^i\partial^\alpha\pi^j\partial^\beta\pi^k. \quad (12)$$

In the above, the first term refers to the direct coupling of the vector meson  $\omega$  to the photon, and hence to the dilepton pairs, as given by the vector dominance model. The decay width of the  $\omega$ -meson in vacuum is dominated by the channel  $\omega \rightarrow 3\pi$ . In the medium, the decay width for  $\omega \rightarrow 3\pi$  is given as

$$\Gamma_{\omega \rightarrow 3\pi} = \frac{(2\pi)^4}{2k_0} \int d^3\tilde{p}_1 d^3\tilde{p}_2 d^3\tilde{p}_3 \delta^{(4)}(P - p_1 - p_2 - p_3) |M_{fi}|^2 \left[ (1 + f(E_1))(1 + f(E_2))(1 + f(E_3)) - f(E_1)f(E_2)f(E_3) \right], \quad (13)$$

where  $d^3\tilde{p}_i = \frac{d^3p_i}{(2\pi)^3 2E_i}$ ,  $p_i$  and  $E_i$ 's are 4-momenta and energies for the pions, and  $f(E_i)$ 's are their thermal distributions. The matrix element  $M_{fi}$  has contributions from the channels  $\omega \rightarrow \rho\pi \rightarrow 3\pi$  (described by Eq. (10) and the direct decay  $\omega \rightarrow 3\pi$  resulting from the contact interaction (second term in (12)) [30, 31, 32]. After fitting  $g_{\omega\rho\pi}$  from the  $\omega \rightarrow \pi\gamma$  decay width, the point interaction coupling  $g_{\omega 3\pi}$  is determined by fitting the partial decay width  $\omega \rightarrow 3\pi$  in vacuum (7.49 MeV) to be 0.24 [20]. The contribution arising from the direct decay is up to around 15 %, which is comparable to the results of [30, 31].

With the modifications of the vector meson masses in the hot and dense medium, the contribution from the decay mode  $\omega \rightarrow \rho\pi$  becomes accessible [8, 20] when  $m_\omega^* > m_\rho^* + m_\pi$ . This is also considered in the present work.

### 3. PARAMETRISATION OF THE PHOTON SELF ENERGY IN THE HADRONIC PHASE

Lattice simulations indicate that QCD undergoes a phase transition at a critical temperature,  $T_c$ , above which there is QGP phase, with quarks and gluons as the relevant degrees of freedom. As one approaches the critical temperature from the above, the quarks and gluons get confined to form the hadrons, which become the effective degrees of freedom for temperatures below  $T_c$ . In this section, we discuss the parametrisation of the photon self energy in the present scenario for the hadronic phase. The photon here couples to the vector mesons ( $\rho$  and  $\omega$ ) and the electromagnetic current-current correlator can be related to the

currents generated by these mesons which are calculated using a Lagrangian describing the hadronic phase. The averaged photon spectral function is defined as [21]

$$R(q) = \frac{12\pi}{q^2} \text{Im}\bar{\Pi}(q), \quad (14)$$

where the photon self energy is related to the sum of the vector meson self energies as

$$\text{Im}\bar{\Pi}(q) = -\frac{1}{3} \sum_V \Pi_\mu^{\mu V}(q). \quad (15)$$

In the limit of  $\vec{q} \rightarrow 0$ , the averaged photon spectral function can be written as

$$R(q) = 12\pi q_0^2 \sum_V \text{Im}\Pi^V(q_0) \equiv 12\pi \sum_V \text{Im}\tilde{\Pi}^V(q_0). \quad (16)$$

In the Walecka model, the vector self energies can be parametrised as a Breit-Wigner distribution with an energy dependent decay width, along with a continuum as [33]

$$\text{Im}\tilde{\Pi}^V(q_0) = f_V^2 \frac{q_0 \Gamma_V(q_0)}{(q_0^2 - m_V^2)^2 + (q_0 \Gamma_V(q_0))^2} + \frac{C_V}{8\pi} \left(1 + \frac{\alpha_s(q_0)}{\pi}\right) \frac{1}{1 + e^{(\omega_0^V - q_0)/\delta}} \quad (17)$$

for the vector mesons,  $V = \rho, \omega$ . In the above,  $f_\rho$  and  $f_\omega$  are the coupling constants corresponding to the vector-meson-photon interactions. The continuum part is described as a smooth function in the energy [34, 35] instead of a step function as is usually adopted in QCD sumrule calculations [16, 36]. The values,  $C_\rho=1$  and  $C_\omega=1/9$  give the correct asymptotic limits for the spectral functions,  $\lim_{q_0 \rightarrow \infty} R_\rho = 3/2$  and  $\lim_{q_0 \rightarrow \infty} R_\omega = 1/6$  [16, 34, 35, 36]. Also, the energy dependence of the strong coupling constant occurring in the meson self energies has been taken into consideration and is given as  $\alpha_s(q_0) = 0.7/\ln(q_0/0.2)$  [34], where  $q_0$  is in units of GeV. The values for the parameters  $\omega_0^{\rho, \omega}$  correspond to the threshold energies above which asymptotic freedom is restored and quark model estimates for cross-sections become valid. The vacuum values for the parameters appearing in the continuum part of the spectral function as derived from the experimental data of  $e^+e^- \rightarrow \text{hadrons}$  are  $\omega_0^\rho = 1.3$  GeV,  $\omega_0^\omega = 1.1$  GeV, and  $\delta = 0.2$  GeV [34]. The vacuum values for the other parameters in the Breit-Wigner part of the photon spectral function are  $f_\rho=152$  MeV,  $f_\omega=50$  MeV,  $m_\rho=770$  MeV,  $m_\omega=783$  MeV,  $\Gamma_\rho=151$  MeV,  $\Gamma_\omega=7.5$  MeV. The masses of the vector mesons are replaced by the medium modified masses including quantum correction effects [20], as a simple pole approximation [36, 37]. However, the energy dependence of the decay widths is considered. We assume the medium modified threshold energies,  $\omega_0^{V*}$  to be given

by the simple scaling [33]  $\frac{\omega_0^{V*}}{\omega_0^V} = \frac{m_V^*}{m_V}$ . The above parametrisation of the photon spectral function for the hadronic phase is used for studying the dynamical evolution of the strongly interacting matter arising in a ultrarelativistic heavy ion collision in an expanding fireball model [21]. In the following section, we briefly discuss the parametrisation of the photon self energy in the QGP phase described by a quasiparticle picture [17].

#### 4. PHOTON SELF ENERGY IN THE QGP PHASE

The QGP phase is described [17] using a quasiparticle picture. The model treats quarks and gluons as massive thermal quasiparticles with their properties determined so as to be compatible with the lattice QCD data. For temperatures much larger than  $T_c$ , the thermal masses can be calculated in the hard thermal loop (HTL) approximation using the perturbative QCD techniques. For temperatures near the phase transition, however, the coupling  $\alpha_s$  becomes large thus invalidating any perturbative techniques. Around  $T_c$ , a power law fall-off is assumed for the thermal masses, based on the conjecture that the phase transition is either weakly first order or second order as indicated by the lattice calculations. The thermodynamic quantities for the QGP are calculated in terms of two functions  $B(T)$  and  $C(T)$  introduced in the model, which account for the thermal vacuum energy and the onset of confinement for temperature approaching  $T_c$ . The quasiparticles are by construction noninteracting and hence the quasiparticle  $q\bar{q}$  becomes the only contribution to the photon self energy [17]. In the QGP phase the time like photon couples to the continuum of thermally excited  $q\bar{q}$  states and subsequently converts into a dilepton pair, which gives the contribution to the dilepton emission rate from the QGP phase.

#### 5. THE FIREBALL EVOLUTION MODEL

In this section, we briefly outline the general framework of the fireball evolution model. The model is described in greater detail in [21].

The underlying assumption of the model is that the strongly interacting matter produced in the initial stage of the collision reaches thermal equilibrium at a timescale  $\tau_0 \approx 1$  fm/c. For simplicity, we assume spatial homogeneity of all thermodynamic parameters throughout a 3-volume at a given proper time. The evolution dynamics is then modelled by calculating the

thermodynamic response to a volume expansion that is consistent with measured hadronic momentum spectra at freeze-out.

The volume itself is taken to be cylindrically symmetric around the beam ( $z$ -)axis. In order to account for collective flow, we boost individual volume elements inside the fireball volume with velocities depending on their position. As flow velocities in longitudinal direction turn out to be close to the speed of light, we have to include the effects of time dilatation. On the other hand, we can neglect the additional time dilatation caused by transverse motion, since typically  $v_{\perp} \ll v_z$ . The thermodynamically relevant volume is then given by the collection of volume elements corresponding to the same proper time  $\tau$ . In order to characterize the volume expansion within the given framework, we need first of all the expansion velocity in longitudinal direction as it appears in the center of mass frame. For the position of the front of the cylinder, we make the ansatz

$$z(t) = v_0 t + c_z \int_{t_0}^t dt' \int_{t_0}^{t'} dt'' \frac{p(t'')}{\epsilon(t'')}, \quad (18)$$

where  $c_z$  is a free parameter. The time  $t$  starts running at  $t_0$  such that  $z_0 = v_0 t_0$  is the initial longitudinal extension with  $v_0$  the initial longitudinal expansion velocity. The longitudinal position  $z(t)$  and  $t$  itself define a proper time curve  $\tau = \sqrt{t^2 - z^2(t)}$ . Solving for  $\tilde{t} = t(\tau)$  one can construct  $\tilde{z}(\tau) = z(\tilde{t})$ . Then the position of the fireball front  $z(t)$  in the center of mass frame can be translated into the longitudinal extension  $L(\tau)$  of the cylinder on the curve of constant proper time  $\tau$ . One obtains

$$L(\tau) = 2 \int_0^{\tilde{z}(\tau)} ds \sqrt{1 + \frac{s^2}{\sqrt{s^2 + \tau^2}}}. \quad (19)$$

At the same proper time we can define the transverse flow velocity and construct the transverse extension of the cylinder as a circle of radius

$$R(\tau) = R_0 + c_{\perp} \int_{\tau_0}^{\tau} d\tau' \int_{\tau_0}^{\tau'} d\tau'' \frac{p(\tau'')}{\epsilon(\tau'')} \quad (20)$$

where  $R_0$  corresponds to the initial overlap radius, and  $c_{\perp}$  is a free parameter. With the values of  $L$  and  $R$  obtained at a given proper time we can parametrize the 3-dimensional volume as

$$V(\tau) = \pi R^2(\tau) L(\tau). \quad (21)$$

In principle the model is fully constrained by fixing the freeze-out time  $t_f$  (at the fireball front), the proper time  $\tau_f$  and the two constants  $c_{\perp}$  and  $c_z$ , such that the measured hadronic

observables are reproduced. In practice this is achieved only at SPS energy, where the freeze-out analysis [38] allows a complete characterization on the basis of hadronic  $dN/dy$  and  $m_t$ -spectra and HBT radii. For the 5% most central Pb-Pb collisions one requires

$$R(\tau_f) = R_f, \quad v_\perp(\tau_f) = v_\perp^f, \quad v_z(\tau_f) = v_z^f \quad \text{and} \quad T(\tau_f) = T_f \quad (22)$$

while making a trial ansatz for the ratio  $p/\epsilon$ . Note that the proportionality of the acceleration to this ratio (which is reminiscent of the behaviour of the speed of sound) allows a soft point in the EoS to influence and delay the volume expansion.

Assuming entropy conservation during the expansion phase, we fix the entropy per baryon from the number of produced particles per unit rapidity. Calculating the number of participant baryons as

$$N_p(b) = \int d^2b' n_p(\mathbf{b}, \mathbf{b}') = \int d^2b' T_A(b') \left[ 1 - \exp(-\sigma_{NN}^{in} T_B(\tilde{b}')) \right] + (T_A \leftrightarrow T_B), \quad (23)$$

with  $T_{A,B}(\mathbf{b}) = \int dz \rho_{A,B}(\mathbf{r})$  the nuclear thickness function,  $\tilde{b}' = |\mathbf{b} - \mathbf{b}'|$  and  $\rho_{A,B}(\mathbf{r})$  the nuclear density distributions of nuclei  $A$  and  $B$  we find the total entropy  $S_0$ . The entropy density at a given proper time is then determined by  $s = S_0/V(\tau)$ . Using the EoS given by the quasiparticle approach [17], thereby providing the link with lattice QCD, we find  $T(s(\tau))$  and also  $p(\tau)$  and  $\epsilon(\tau)$ , which in the next iteration replace the trial ansatz in the volume parametrization. Finally we arrive at a thermodynamically self-consistent model for the fireball which is by construction able to describe the hadronic momentum spectra at freeze-out.

Thus, the fireball evolution is completely constrained by hadronic observables. In [21], it has been shown that this scenario is able to describe the measured spectrum of low mass dileptons, and in [39] it has been demonstrated that under the assumption of statistical hadronization at the phase transition temperature  $T_C$ , the measured multiplicities of hadron species can be reproduced. In [40], the model has been shown to describe charmonium suppression correctly. None of these quantities is, however, very sensitive to the detailed choice of the equilibration time  $\tau_0$ . Therefore, we have only considered the ‘canonical’ choice  $\tau_0 = 1$  fm/c so far. The calculation of photon emission within the present framework provides the opportunity to test this assumption and to limit the choice of  $\tau_0$ . In [41], this has been investigated in some detail. Within the present framework, the limits  $0.5 \text{ fm/c} < \tau_0 < 3 \text{ fm/c}$  could be found. Variations within these limits, however, do not affect the spectrum of dileptons with invariant mass below 1 GeV significantly.

## 6. DILEPTON EMISSION

The emission of dileptons in the model is calculated using the differential emission rate

$$\frac{dN}{d^4x d^4q} = \frac{\alpha^2}{\pi^3 q^2} \frac{1}{e^{\beta q^0} - 1} \text{Im}\bar{\Pi}(q, T) = \frac{\alpha^2}{12\pi^4} \frac{R(q, T)}{e^{\beta q^0} - 1}, \quad (24)$$

where  $\alpha = e^2/4\pi$  and we have neglected the lepton masses. Eq.(24) is valid to order  $\alpha$  in the electromagnetic interaction and to all orders in the strong interaction. Its main ingredient is the temperature-dependent spectral function  $R(q, T)$ .

The differential rate of eq.(24) is integrated over the space-time history of the collision to compare the calculated dilepton rates with the CERES/NA45 data [1] taken in Pb-Au collisions at 158 AGeV (corresponding to a c.m. energy of  $\sqrt{s} \sim 17$  AGeV) and 40 AGeV ( $\sqrt{s} \sim 8$  AGeV). The CERES experiment is a fixed-target experiment. In the lab frame, the CERES detector covers the limited rapidity interval  $\eta = 2.1 - 2.65$ , *i.e.*  $\Delta\eta = 0.55$ . We integrate the calculated rates over the transverse momentum  $p_T$  and average over  $\eta$ , given that  $d^4p = M p_T dM d\eta dp_T d\theta$ . The formula for the space-time- and  $p$ -integrated dilepton rate hence becomes

$$\frac{d^2 N}{dM d\eta} = \frac{2\pi M}{\Delta\eta} \int_{\tau_0}^{\tau_f} d\tau \int d\eta V(\eta, T(\tau)) \int_0^\infty dp_T p_T \frac{dN(T(\tau), M, \eta, p_T)}{d^4x d^4p} \text{Acc}(M, \eta, p_T), \quad (25)$$

where  $\tau_f$  is the freeze-out proper time of the collision,  $V(\eta, T(\tau))$  describes the proper time evolution of volume elements moving at different rapidities and the function  $\text{Acc}(M, \eta, p_T)$  accounts for the experimental acceptance cuts specific to the detector. At the CERES experiment, each electron/positron track is required to have a transverse momentum  $p_T > 0.2$  GeV, to fall into the rapidity interval  $2.1 < \eta < 2.65$  in the lab frame and to have a pair opening angle  $\Theta_{ee} > 35$  mrad. Finally, for comparison with the CERES data, the resulting rate is divided by  $dN_{ch}/d\eta$ , the rapidity density of charged particles.

As in [21], we also include the effects of the overpopulation of the pion phase space due to decay processes of heavy resonances to the emission from hadronic matter by introducing a temperature-dependent pion chemical potential  $\mu_\pi(T)$ .

In addition to the thermal emission of dileptons, we also consider dileptons from vacuum decays of vector mesons after the thermal decoupling of the fireball and hard dileptons from initial Drell-Yan processes. For details of the calculation of these contributions see ref. [21].

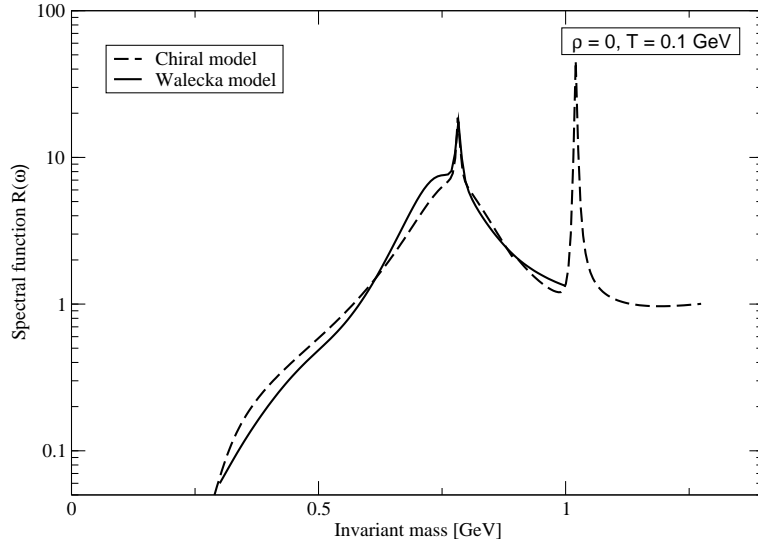


FIG. 1: Photon spectral function at  $T=100$  MeV.

A final remark: The spectral function considered in the present work is only available below 1 GeV invariant mass range. Therefore, we do not include thermal emission of dileptons from hadronic matter above that scale when discussing the Walecka model results. This leads to small differences between the two approaches for large invariant masses. This region, however, is not dominantly filled by emission from the hadronic phase but by the QGP and Drell-Yan contribution.

## 7. RESULTS AND DISCUSSIONS

We now discuss the results obtained for the photon spectral function in the hadronic matter arising due to medium modification of the vector mesons with the quantum correction effects from baryons and scalar mesons, and its effect on the dilepton emission spectra. In the present investigation, we choose the renormalised sigma meson self interaction coupling  $\lambda_R$  to be 5, corresponding to the value of incompressibility of nuclear matter to be 329 MeV [20]. As stated earlier, the dilepton spectra are studied in a mixed scenario of QGP and hadronic matter using the fireball model as described in the previous section. The photon spectral function as obtained in the present hadronic scenario is compared with the earlier calculation obtained in a chiral SU(3) model [16]. The spectral functions in both the models are shown in figure 1 for vanishing baryon density and a temperature of 100 MeV. As expected due to absence of any pronounced medium effects for this temperature, the two

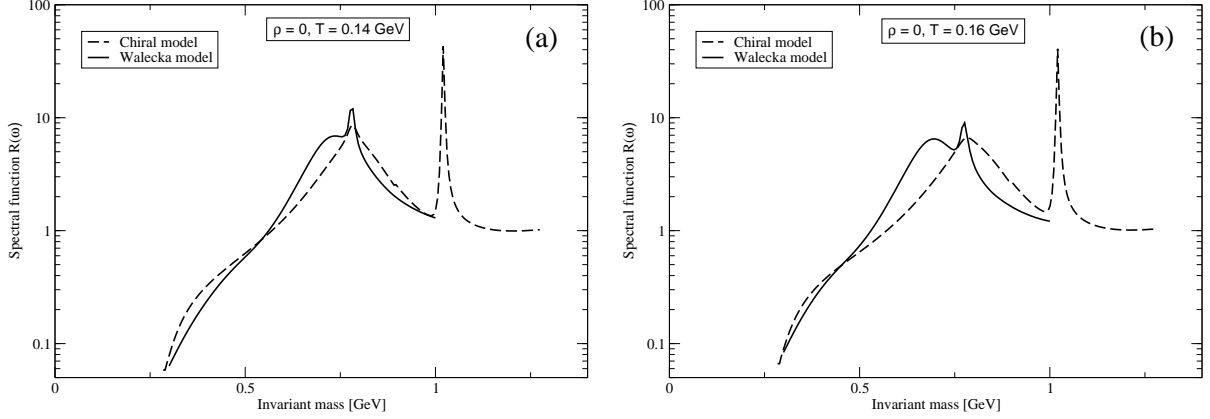


FIG. 2: Photon spectral function at  $T=140$  MeV and  $T=160$  MeV.

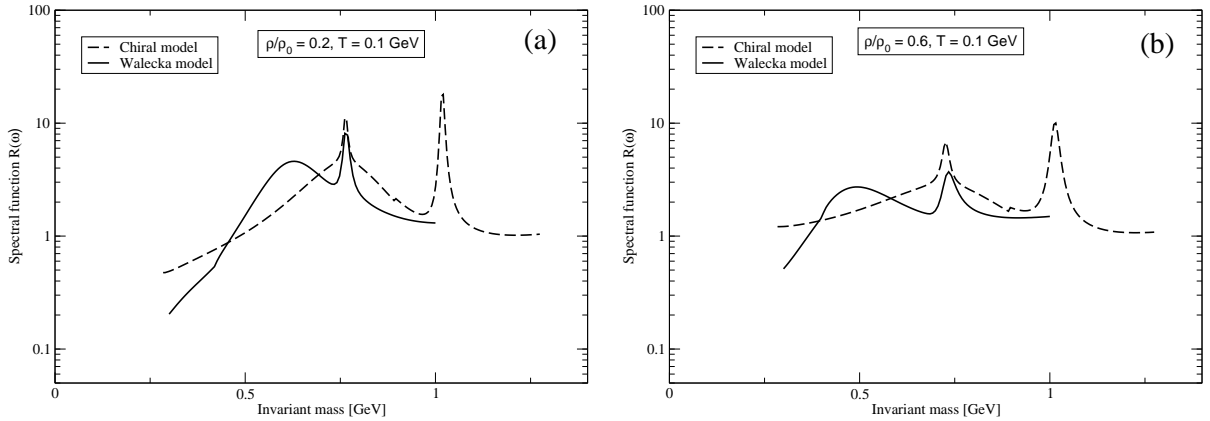


FIG. 3: Photon spectral function at  $T=100$  MeV and at densities  $0.2\rho_0$  and  $0.6\rho_0$ , with  $\rho_0=0.17$   $fm^{-3}$ .

models yield similar results.

In figure 2, the temperature dependence of the photon spectral function is shown. The spectral function in the present hadronic scenario is seen to develop a distinct  $\rho$  peak at higher temperatures. This is a reflection of the fact that with quantum correction effects, the  $\rho$ -mass, due to the tensorial coupling, has a larger drop as compared to the mass of the  $\omega$ -meson. In the present calculations, the effect of temperature on the  $\rho$ -mass is rather moderate up to around a temperature of 160 MeV or so. This is in line with the previous calculation of [42]. The broadening of the  $\rho$  peak at higher temperature takes place as the Bose enhancement dominates over the effect of drop in  $\rho$ -mass, leading to an increase in the  $\rho$  decay width. On the other hand, the density dependence of the  $\rho$  mass is seen to be

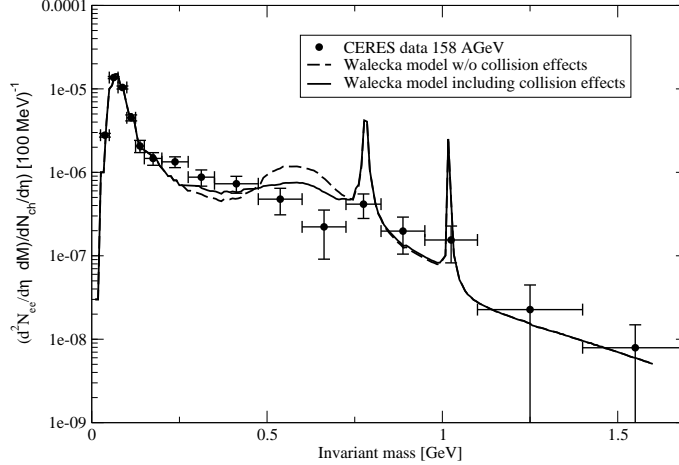


FIG. 4: Dilepton emission rate for 158 AGeV at SPS for the Walecka model with and without the collision effects.

quite significant [20] which leads to the  $\rho$  peak position shifted to lower values in the present calculation as illustrated in figure 3. The mass of the  $\rho$ -meson remains almost unchanged in the chiral model, whereas the  $\rho$ -decay width has appreciable enhancement in the medium due to inelastic processes, like  $\rho N \rightarrow \pi N$ ,  $\rho N \rightarrow \pi \Delta$ , and also, from  $\rho N \rightarrow \omega N$  at higher energies. This basically leads to the  $\rho$  peak to be completely dissolved in the chiral model [16], leaving only a broad continuum. In the absence of collisional effects, the decay width for  $\rho$  arises from the process  $\rho \rightarrow \pi\pi$ . Here, the Bose-Einstein factors in (5) have the effect of increasing the width in the thermal medium, whereas the stronger dropping of the  $\rho$ -mass in the medium at higher densities in the present calculations has the opposite effect of decreasing the decay width and overcompensates the effect from the Bose enhancement factor. The collisional effects lead to considerable flattening of the spectral function for the  $\rho$  peak.

Figures 4 and 5 show the dilepton spectra using the fireball model in the present hadronic scenario and a quasiparticle picture for QGP. The inclusion of collisional effects due to scattering off by the nucleons is seen to lead to considerable broadening of the  $\rho$ -peak in the dilepton spectra. The difference is seen to be more prominent for SPS 40 AGeV corresponding to a higher baryon density. The present hadronic scenario leads to a distinct structure in the dilepton emission rate due to the undissolved  $\rho$  peak in the absence of the contribution from the  $\rho N$  scattering processes, which is seen to be flattened due to these collision processes. The dropping of the vector meson masses in QHD in the relativistic

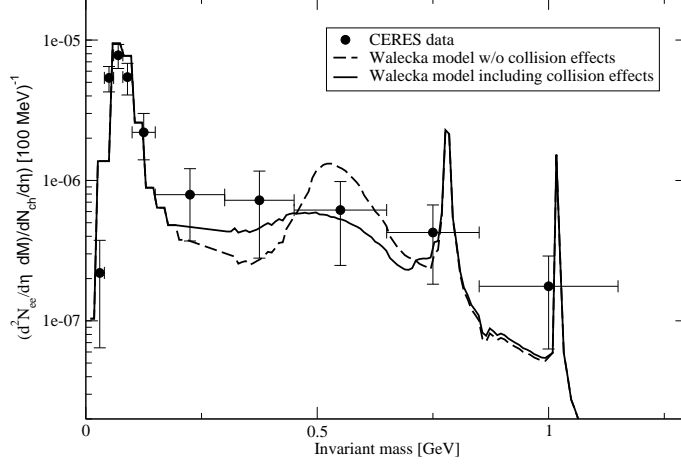


FIG. 5: Dilepton emission rate for 40 AGeV at SPS for the Walecka model with and without the collision effects.

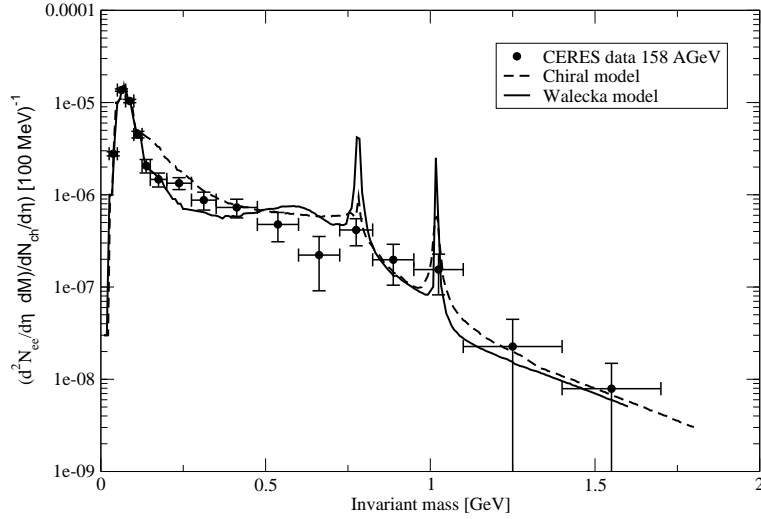


FIG. 6: Dilepton emission rate for 158 AGeV at SPS for the chiral and Walecka models.

Hartree approximation [43] also has been seen to yield similar results. In the absence of collisional processes, the drop in the  $\rho$  mass leads to enhancement in the dilepton yield below the vacuum  $\rho$  mass, but does not have the rather flat structure as observed in the data. Inclusion of inelastic processes  $\rho N \rightarrow \pi N$ ,  $\rho N \rightarrow \pi \Delta$ ,  $\rho N \rightarrow \omega N$ , give rise to considerable broadening of the spectra below the vacuum  $\rho$ -mass.

Figures 6 and 7 compare the dilepton emission rates of the present investigation to the results of chiral model description for hadronic matter as well as to the results from SPS, 158 AGeV and SPS, 40 AGeV 30% central Pb+Au collision. It may be noted that the fire-

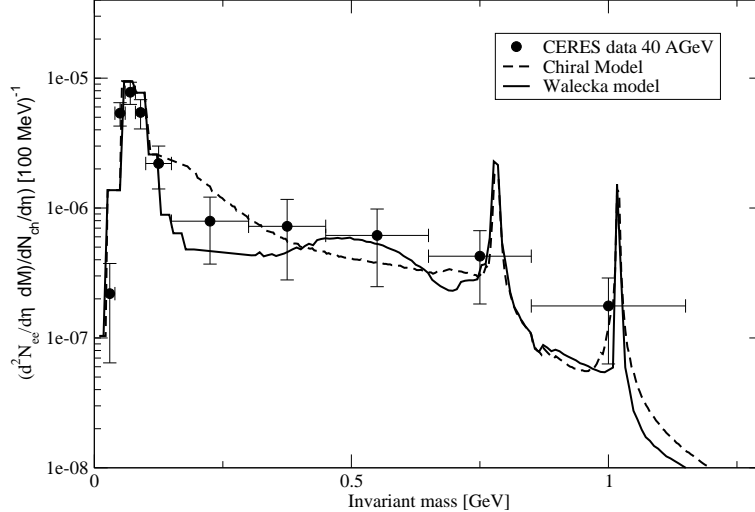


FIG. 7: Dilepton emission rate for 40 AGeV at SPS for the chiral and Walecka models.

ball evolution, detector acceptance, contributions from the QGP and Drell-Yan background were modelled exactly in the same way for both theoretical curves. The previous hadronic scenario based on a chiral model [16] has the observed dissolved  $\rho$  peak arising due to the Bose enhancement factors as well as the inelastic channels. In the present calculations, the collisions by nucleons lead to significant broadening of the  $\rho$ -peak in the dilepton spectra.

## 8. SUMMARY

To summarize, we have investigated here the medium properties of the vector mesons in the Walecka model including the vacuum polarization effects and their effects on the dilepton spectra using a fireball model. The density dependence of the vector meson properties are seen to be the dominant medium effect as compared to the temperature dependence. We have considered a mixed scenario of QGP and hadronic matter [21] and have compared the dilepton emission rates of the present calculations to those from a previous calculation using a chiral SU(3) model, as well as to the experimental results from SPS at 158 AGeV and 40 AGeV.

Since the evolution of the fireball was not in any way adjusted to the dilepton data but rather fixed from different observables, we are in a position to compare the different spectral functions with the data without being subject to large uncertainties regarding the medium

evolution.

When the scattering due to nucleons is not taken into account in the present calculations, there is a more pronounced difference in the two models for SPS, 40 AGeV, as compared to SPS, 158 AGeV due to the higher baryon density. However, there is seen to be significant broadening of the spectra due to these collision effects within the present investigation.

### Acknowledgments

One of the authors (AM) would like to thank J. Reinhardt and S. Schramm for fruitful discussions. AM is grateful to the Institut für Theoretische Physik for warm hospitality and acknowledges financial support from Bundesministerium für Bildung und Forschung (BMBF). TR would like to thank W. Weise and R. A. Schneider for their support of this work. Financial support was given in part by BMBF and GSI.

- 
- [1] N. Masera for the HELIOS-3 collaboration, Nucl. Phys. **A 590**, 93c (1995); G. Agakichiev et al (CERES collaboration), Phys. Rev. Lett. **75**, 1272 (1995); G. Agakichiev et al (CERES collaboration), Phys. Lett. **B 422**, 405 (1998); G. Agakichiev et al (CERES collaboration), Nucl. Phys. **A 661**, 23c (1999); R. J. Porter et al (DLS collaboration), Phys. Rev. Lett. **79**, 1229 (1997); W. K. Wilson et al (DLS collaboration), Phys. Rev. C **57**, 1865 (1998).
  - [2] D. P. Morrison (PHENIX collaboration), Nucl. Phys. **A 638**, 565c (1998); J. Stroth (HADES collaboration), Advances Nuclear Dynamics **5**, 311 (1999).
  - [3] G. E. Brown and M. Rho, Phys. Rev. Lett. **66**, 2720 (1991).
  - [4] T. Hatsuda and Su H. Lee, Phys. Rev. **C 46**, R34 (1992); T. Hatsuda, S. H. Lee and H. Shiomi, Phys. Rev. **C 52**, 3364 (1995); X. Jin and D. B. Leinweber, Phys. Rev. **C 52**, 3344 (1995); T. D. Cohen, R. D. Furnstahl, D. K. Griegel and X. Jin, Prog. Part. Nucl. Phys. **35**, 221 (1995); R. Hofmann, Th. Gutsche, A. Faessler, Eur. Phys. J. **C 17**, 651 (2000); S. Mallik and K. Mukherjee, Phys. Rev. **D 58**, 096011 (1998); S. Mallik and A. Nyffeler, Phys. Rev. **C 63**, 065204 (2001); C. Ernst, S. A. Bass, M. Belkacem, H. Stöcker and W. Greiner, Phys. Rev. **C 58**, 447 (1998).
  - [5] H. Shiomi and T. Hatsuda, Phys. Lett. **B 334**, 281 (1994).

- [6] T. Hatsuda, H. Shiomi and H. Kuwabara, Prog. Theor. Phys. **95**, 1009 (1996).
- [7] H.-C. Jeans, J. Piekarewicz and A. G. Williams, Phys. Rev. **C 49**, 1981 (1994); K. Saito, K. Tsushima, A. W. Thomas, A. G. Williams, Phys. Lett. **B 433**, 243 (1998).
- [8] Jan-e Alam, S. Sarkar, P. Roy, B. Dutta-Roy and B. Sinha, Phys. Rev. **C 59**, 905 (1999).
- [9] R. Rapp and J. Wambach, Adv. Nucl. Phys. **25**, 1 (2000).
- [10] C. M. Ko, V. Koch and G. Q. Li, Ann. Rev. Nucl. Sci. **47**, 505 (1997).
- [11] Jan-e Alam, P. Roy, S. Sarkar and B. Sinha, nucl-th/0106038; Jan-e Alam, S. Sarkar, P. Roy, T. Hatsuda and B. Sinha, Ann. Phys. **286**, 159 (2000); F. Karsch, E. Laermann, P. Petreczky, S. Stickan, I. Wetzorke, hep-lat/0110208.
- [12] K. Redlich, J. Cleymans, V. V. Goloviznin, in Proceedings on NATO Advanced Workshop on Hot Hadronic Matter: Theory and Experiment, N.Y. Plenum Press, 1995, 562p; A. Dumitru, D. H. Rischke, Th. Schönfeld, L. Winkelmann, H. Stöcker and W. Greiner, Phys. Rev. Lett. **70**, 2860 (1993); P. Jaikumar, R. Rapp and I. Zahed, hep-ph/0112308; Song Gao, Ru-Keng Su, Xue-Qian Li, Comm. Theor. Phys. **28**, 207 (1997); D. Dutta, K. Kumar, A. K. Mohanty, R. K. Choudhury, Phys. Rev. **C 60**, 014905, 1999.
- [13] G. Q. Li, C. M. Ko and G. E. Brown, Phys. Rev. Lett **75**, 4007 (1995); G. Q. Li, C. M. Ko and G. E. Brown, Nucl. Phys. **A 606**, 568 (1996); G. Q. Li, C. M. Ko, G. E. Brown and H. Sorge, Nucl. Phys. **A 611**, 539 (1996).
- [14] E. L. Bratkovskaya and W. Cassing, Nucl. Phys. **A 619**, 413 (1997).
- [15] R. Rapp, G. Chanfray and J. Wambach, Phys. Rev. Lett. **76**, 368 (1996); R. Rapp, G. Chanfray and J. Wambach, Nucl. Phys. **A 661**, 472 (1997).
- [16] F. Klingl, N. Kaiser and W. Weise, Nucl. Phys. **A 624**, 527 (1997).
- [17] R. A. Schneider and W. Weise, Phys. Rev. **C 64**, 055201 (2001).
- [18] A. Mishra, P. K. Panda, S. Schramm, J. Reinhardt and W. Greiner, Phys. Rev. **C 56**, 1380 (1997).
- [19] A. Mishra, J. C. Parikh and W. Greiner, Jour. Phys. **G 28**, 151 (2002).
- [20] A. Mishra, J. Reinhardt, H. Stoecker and W. Greiner, Phys. Rev. **C 66**, 064902 (2002).
- [21] T. Renk, R. A. Schneider and W. Weise, Phys. Rev. **C 66**, 014902 (2002); T. Renk, Ph.D. Thesis.
- [22] A. Mishra and H. Mishra, J. Phys. **G 23**, 143 (1997); S.Y. Pi and M. Samiullah, Phys. Rev. **D 36**, 3121 (1987); G. A. Camelia and S.Y. Pi, Phys. Rev. **D 47**, 2356 (1993); A. Mishra and

- H. Mishra, J. Phys. **G 23**, 143 (1997).
- [23] A. Mishra, P. K. Panda and W. Greiner, Jour. Phys. **G 27**, 1561 (2001).
- [24] A. Mishra, P. K. Panda and W. Greiner, Jour. Phys. **G 28**, 67 (2002).
- [25] H. Umezawa, H. Matsumoto and M. Tachiki, *Thermofield Dynamics and Condensed States* (North-Holland, Amsterdam, 1982).
- [26] B. D. Serot and J. D. Walecka, Adv. Nucl. Phys. **16**, 1 (1986); S. A. Chin, Ann. Phys. **108**, 301 (1977); S. Pal, Song Gao, H. Stöcker and W. Greiner, Phys. Lett. **B 465**, 282 (1999).
- [27] M. Asakawa, C. M. Ko, P. Levai and X. J. Qiu, Phys. Rev. **C 46**, R1159 (1992); M. Herrmann, B. L. Friman and W. Nörenberg, Nucl. Phys. **A 560**, 411 (1993); G. Chanfray and P. Shuck, Nucl. Phys. **A 545**, 271c (1992).
- [28] W. Grein, Nucl. Phys. **B 131**, 255 (1977); W. Grein and P. Kroll, Nucl. Phys. **A 338**, 332 (1980).
- [29] J. J. Sakurai, *Currents and Mesons* (The University of Chicago Press, Chicago, 1969); M. Gell-Mann, D. Sharp, and W. D. Wagner, Phys. Rev. Lett. **8**, 261 (1962).
- [30] B. A. Li, Phys. Rev. **D 52**, 5165 (1995).
- [31] F. Klingl, N. Kaiser and W. Weise, Z. Phys. **A 356**, 193 (1996).
- [32] Ö. Kaymakçalan, S. Rajeev and I. Schechter, Phys. Rev. **D 30**, 594 (1984).
- [33] J. Alam, S. Sarkar, P. Roy, T. Hatsuda, B. Sinha, Ann. Phys. **286**, 159, 2000.
- [34] E. V. Shuryak, Rev. Mod. Phys. **65**, 1 (1993).
- [35] J. I. Kapusta and E. V. Shuryak, Phys. Rev. **D 49**, 4694 (1994).
- [36] T. Hatsuda and S. H. Lee, Phys. Rev. **C 46**, R34 (1992).
- [37] J. Alam, S. Sarkar, P. Roy, B. Dutta-Roy, B. Sinha, Phys. Rev. **C 59**, 905 (1999).
- [38] B. Tomasik, U. A. Wiedemann and U. W. Heinz, nucl-th/9907096.
- [39] T. Renk, hep-ph/0210307.
- [40] A. Polleri, T. Renk, R. Schneider and W. Weise, nucl-th/0306025.
- [41] T. Renk, Phys. Rev. **C 67** (2003) 064901.
- [42] C. Gale and J. I. Kapusta, Nucl. Phys. **B 357**, 65 (1991).
- [43] S. Sarkar, Jan-e Alam and T. Hatsuda, nucl-th/0011032.